**Title**
A Three Dimensional Finite Difference Time Domain Sub-Gridding Method



**Author**
Luong, Kevin Quy Tanh

**Publication Date**
2019

Peer reviewed|Thesis/dissertation

UNIVERSITY OF CALIFORNIA

Los Angeles

# A Three Dimensional Finite Difference Time Domain Sub-Gridding Method

A thesis submitted in partial satisfaction

of the requirements for the degree Master of Science

in Electrical and Computer Engineering

by

Kevin Quy Tanh Luong

2019

ABSTRACT OF THE THESIS

A Three Dimensional Finite Difference

Time Domain Sub-Gridding Method

by

Kevin Quy Tanh Luong

Master of Science in Electrical and Computer Engineering

University of California, Los Angeles, 2019

Professor Yuanxun Ethan Wang, Chair

The finite difference time domain method has long been one of the most widely used numerical methods for solving Maxwell's equations due in part to its accuracy, explicit nature, and simplicity of implementation. Modern research interests have created a need for this method to be extended to handle multi-scale multi-physics problems where numerous physical phenomena are coupled with classical electrodynamics. These phenomena typically occur on vastly different spatial scales; however, the conventional finite difference time domain method requires a uniform spatial discretization across the entire simulation space. Additionally, the maximum time evolution that may be solved in a single iteration of the algorithm is proportional to the smallest discretization length. Consequently, properly resolving the smallest feature of a multi-scale problem causes phenomena of a larger scale to be over-resolved, resulting in an

unnecessarily large amount of memory and often an impractical number of computations required for simulation. The development of a capability for sub-gridding, where local domains of fine resolution may be incorporated into a simulation space of coarser resolution, is imperative to treat this issue. This thesis proposes a new algorithm to implement sub-gridding. The results of comprehensive numerical evaluations show promise for this algorithm to be of general use in solving multi-scale multi-physics problems.

The thesis of Kevin Quy Tanh Luong is approved.

Tatsuo Itoh

Yahya Rahmat-Samii

Yuanxun Ethan Wang, Committee Chair

University of California, Los Angeles

2019

# TABLE OF CONTENTS

# LIST OF FIGURES

# CHAPTER 1

# Introduction

## 1.1 Research Background

### 1.1.1 Numerical Electromagnetics

Electrostatic and magnetostatic phenomena were first observed in ancient Greece as curious behaviors of amber and lodestone respectively. Progress in understanding these phenomena was slow for a long time leading up to Charles-Augustin de Coulomb publishing his inverse-square law for the force between charged particles in 1785 [1]. Coulomb's Law (1-1) marked the beginning of classical electromagnetic theory, which was further developed in the years to follow through a great deal of study among a large number of scientists and mathematicians.

$$\vec{F} = \frac{1}{4\pi\epsilon}\frac{q_1 q_2}{r^2}\hat{r} \tag{1-1}$$

All the research done was ultimately unified in 1864 by James Clerk Maxwell in his paper, *A Dynamical Theory of the Electromagnetic Field* [1]. This paper presented a single set of equations, known now as Maxwell's Equations (1-2), completely describing the classical theory of electromagnetic fields.

$$\nabla \times \vec{E} = -\frac{\partial \vec{B}}{\partial t} \tag{1-2a}$$

$$\nabla \times \vec{H} = \frac{\partial \vec{D}}{\partial t} + \vec{J} \tag{1-2b}$$

$$\nabla \cdot \vec{D} = \rho \tag{1-2c}$$

$$\nabla \cdot \vec{B} = 0 \tag{1-2d}$$

With the foundational physics established, application-oriented research blossomed, leading to unforetold developments that are now integral parts of modern life. Maxwell's equations today are still just as significant as ever and constitute the core of electrical engineering; solving these equations for any given electrical system of interest provides virtually all that can be known regarding the electromagnetic fields and their behaviors.

The completeness of Maxwell's equations as well as their elegant form are misleading however, as it turns out that they are too complex to solve for most problems of practical interest. Workarounds for this issue were few until around the 1950s when high speed computing finally made numerical methods feasible [2]. Numerical methods are approximate means of solving the equations describing a given problem, involving computation to generate a numeric solution. This is in contrast to analytical methods which involve symbolic manipulation of equations to generate a symbolic solution. Numerical methods were not a new concept at the time; they were simply rarely used due to the fact that they involve an immense volume of computations. Developments in high speed computing caused a resurgence of interest however, allowing for such computations to be handled much more efficiently. Today the numerical evaluation of equations describing a practical problem, or in other words "simulation", has become a mainstay in any research workflow.

Numerical methods solving the frequency domain form of Maxwell's equations were the first to see extensive application and development. Most prevalent were the finite element method, the usage of which began in the 1950s, and the method of moments, which was

introduced around the 1960s [3]. The finite element method is a means of computationally applying variational or weighted residual techniques to solve an equation. The method of moments is based on similar techniques, but typically refers specifically to the evaluation of integral equations involving Green's functions [3]. These methods alone were not sufficient to treat all electromagnetic problems of interest however due to inherent limitations including difficulty in accounting for nonlinear phenomena or the need to solve large sets of linear equations. The gaps in applicability of these methods were addressed by the finite difference time domain (FDTD) method which, though first proposed in the 1960s, did not gain popularity until much later [4]. This method solves the time domain form of Maxwell's equations using finite difference approximations for derivatives. The three methods introduced remain standards for electromagnetic simulation today. While no single method is superior to the others, the problems of interest in this thesis encourage a focus on the FDTD method.

### 1.1.2 Multi-Scale Simulations

One prevalent class of simulations frequently occurring in practice is that of "multi-scale simulations", which derives its name from the fact that multiple spatial scales are required to model both small and large features simultaneously. The problems requiring electromagnetic multi-scale simulations have been widespread. Historically, these have included anything from the coupling of incident fields on aircraft to small scale internal circuitry [20], the operation of waveguides with discontinuity features that are small compared to the waveguide dimensions [21], or the absorption of fields in the human body due to small electronic radiators as part of body area networks [42]. Electromagnetic multi-scale problems will likely always continue to emerge, making this class of simulations of utmost importance.

The current state of technology and research has assigned an even greater significance to multi-scale simulations however. While the aforementioned problems have more or less involved solely electromagnetics, there is massive interest in what are known as "multi-physics" problems in which phenomena from multiple areas of physics are explicitly coupled. Typically, these different physical phenomena occur on disparate spatial scales, meaning that multi-scale and multi-physics problems go hand in hand. In photonics research for example, it is of vital importance to model as accurately as possible the interaction of light with materials. To accomplish this, quantum physics is often coupled with classical electrodynamics [5], requiring the resolution of very different spatial scales. One particular instance of such coupling is with simulations of surface enhanced Raman spectroscopy (SERS). As shown in Figure 1.1, this spectroscopy involves analyte molecules adsorbed onto metal nanoparticles and evaluated based on their interaction with incident light [6]. Modeling the SERS procedure is contingent upon the incorporation of both classical electrodynamics for the light-nanoparticle interaction as well as quantum theory for the light-molecule interaction [5]. The operation of devices based on magnetic materials is another multi-physics, multi-scale problem. Frequency selective limiters for example possess unique behaviors due to the phenomena of electromagnetic field coupling to magnetic spin waves [7]. While the electromagnetic wavelength of operation is typically on the order of centimeters, modeling the spin waves requires accounting for the exchange interaction between magnetic dipoles of the material, requiring resolution on the order of nanometers. Spin waves are visualized in Figure 1.2.

Though the FDTD method lends itself well to the incorporation of physical phenomena beyond electromagnetics, it is not suited to handle multiple spatial scales. Attempts to run multi-scale simulations applying this method tend to involve enormous amounts of memory and

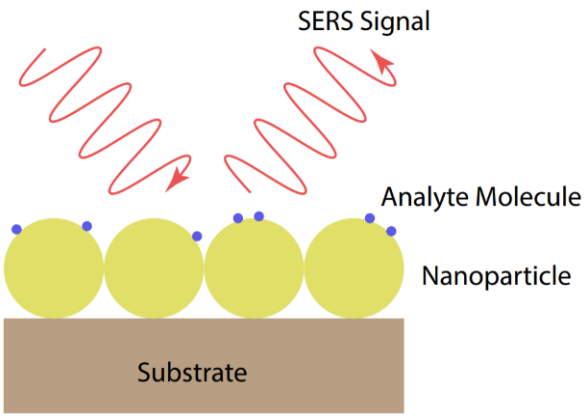


Figure 1.1: Surface enhanced Raman spectroscopy.

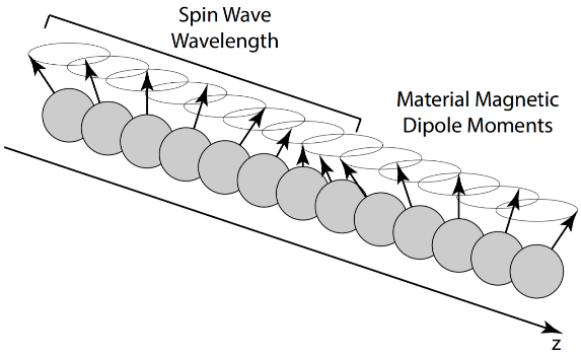


Figure 1.2: Spin wave.

computation, due partially to the fact that uniform discretization of the simulation space is required. In other words, the FDTD method interprets continuous space as a set of discrete points according to a user defined mesh where the same mesh used to resolve small features must also be used for large features. This causes an over-resolution of the large features where, because the field value at each discrete point must be solved as well as stored, memory and computation are drastically increased. The FDTD method also involves discretization in the temporal domain with iterative solving to advance the solution in time. In order to maintain stability of the simulation, the distance between discrete time points is inherently limited to a maximum value

proportional to the smallest distance between discrete space points. Thus, the number of iterations to simulate a system to a given time evolution is inversely proportional to the smallest feature of interest. Clearly, with multi-scale problems this limitation further compounds the large computational requirement.

## 1.2 Research Outline and Goals

The most effective means of addressing the poor multi-scale capabilities of the FDTD method is with a modification of the method that allows for local domains possessing time and space discretizations independent from the rest of the simulation domain. Such a procedure is commonly referred to as "sub-gridding" and its benefits in terms of improving the suitability of the conventional FDTD method for a greater range of problems have been long recognized. Nevertheless, past attempts at implementation have all been lacking in a number of critical characteristics, preventing any particular sub-gridding algorithm from seeing widespread success. The goal of the research in this thesis is to formulate and assess a new sub-gridding algorithm that has greater potential for general applicability than those of past literature.

In Chapter 2, the fundamental principles, advantages, and limitations of the FDTD method are presented. Several means of overcoming these limitations to allow for more efficient multi-scale simulations are then briefly discussed with a focus on why sub-gridding is the most appropriate. This is followed by a comprehensive examination of past attempts to realize a general sub-gridded FDTD method along with a discussion of why none of them have been widely adopted. In Chapter 3, a new sub-gridding algorithm is proposed, and the steps for its implementation are enumerated. In Chapter 4, various numerical tests are performed applying the

algorithm to validate its results and assess its capabilities. Finally, Chapter 5 presents future work that still needs to be done to obtain a further improved sub-gridded FDTD method.

# CHAPTER 2

# The FDTD Method and Multi-Scale Simulations

## 2.1 Introduction to the FDTD Method

### 2.1.1 Overview of the Method

The finite difference time domain method, proposed by Kane Yee in 1966 [8], is a numerical method for solving Maxwell's equations. As implied by its name, this method involves solving the partial differential time domain Maxwell's curl equations using a central finite difference approximation for the derivatives. The derivative for a function of one variable is defined in (2-1). A central finite difference approximates this derivative using a finite $\Delta x$, where the values of the function used in the difference are centered about the original point at which the derivative is to be solved.

$$f'(x) = \lim_{\Delta x \to 0} \frac{f(x + \Delta x) - f(x)}{\Delta x} \tag{2-1}$$

Considering an x-polarized, z-directed plane wave propagating in free space, the FDTD expressions can be derived from (1-2a) and (1-2b) and are given by (2-2a) and (2-2b).

$$E_x|_i^{n+1} = E_x|_i^n + \left(\frac{\Delta t}{\epsilon_0 \Delta z}\right)\left(-\left(H_y|_{i+1/2}^{n+1/2} - H_y|_{i-1/2}^{n+1/2}\right) - \Delta z J_x|_i^{n+1/2}\right) \tag{2-2a}$$

$$H_y|_{i+1/2}^{n+3/2} = H_y|_{i+1/2}^{n+1/2} + \left(\frac{\Delta t}{\mu_0 \Delta z}\right)\left(-(E_x|_{i+1}^{n+1} - E_x|_{i-1}^{n+1})\right) \tag{2-2b}$$

In these equations $\Delta z$ and $\Delta t$ represent the distances between discrete points in the spatial and temporal domains at which the fields are solved. Additionally, *i* and *n* are integers used to represent specific points in time and space according to the shorthand given by (2-3).

$$E_x|_i^n = E_x\big(i(\Delta z), n(\Delta t)\big) \tag{2-3}$$

The use of finite differences to approximate derivatives was in no way a novel concept and its origin can be traced as far back as Euler in 1768 [9]. The revolutionary idea of Yee's method was that of staggering the discrete space and time points where the electric and magnetic field component values were solved such that they were not collocated. This is illustrated in Figure 2.1 with a unit cell of the spatial mesh labeled with electric and magnetic field components. A general simulation space using the FDTD method would be comprised of a number of these cells stacked adjacent to each other, sharing faces and edges. The staggered locations at which the fields are solved in time are visualized in Figure 2.2. In this case it is not necessary to distinguish between different components as all are evaluated at the same points in time for a given field.

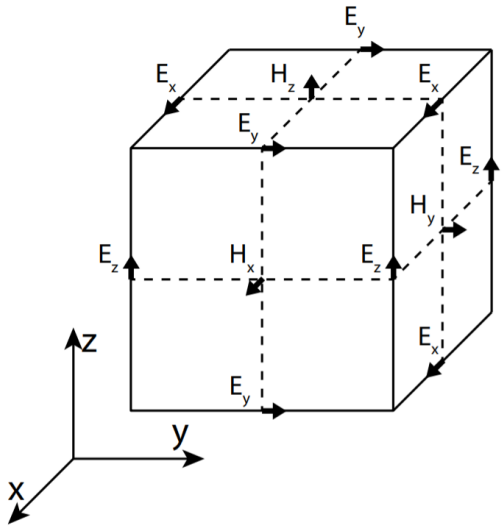


Figure 2.1: Yee unit cell.

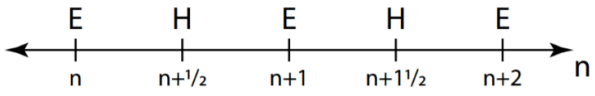


Figure 2.2: Time staggering scheme.

Slowly, as the capabilities of computers continued to improve, Yee's method grew in popularity. It is now the standard for time domain electromagnetic simulations.

### 2.1.2 Advantages of the Method

The irreplaceability of this method for solving Maxwell's equations stems from several of its characteristics [4]. Most obviously, as compared to the method of moments or the finite element method, the FDTD method solves in the time domain. This allows for natural treatment of wideband solutions as well as nonlinear modeling. Another advantage is that this method is explicit, making it much more capable at handling problems involving a large number of unknowns without having to deal with the issues that come with matrix inversion. Furthermore, formulation and modification of the FDTD algorithm itself for a given problem is very simple and straightforward, making the method well suited for research applications. Not only is it almost trivial to alter the geometries of modeled objects, but also the incorporation other phenomena from frequency dependent materials to lumped elements to additional physics is readily accomplished. Unlike other methods, there is no need to modify Green's functions or integral equations to account for these phenomena; rather, the finite difference nature of this method necessitates only the modification of algebraic equations. All of these advantages contribute to the focus on this method for multi-scale multi-physics problems.

### 2.1.3 Limitations of the Method

Though certainly possessing many advantageous characteristics, the FDTD method is not without its own drawbacks and limitations [10]. One of such drawbacks is the fact that the entire simulation space must be discretized according to some mesh regardless of whether field

component values at any given location are part of the desired solution or not. This results in an excessive increase in both computation and memory to solve for and store all these component values respectively. Figure 2.3 shows a two dimensional cross section of a microstrip patch antenna. In order to simulate the radiation from this antenna, all aspects of its structure as well as the free space surrounding it must be meshed. The amount of free space meshed is dependent on how the boundary of the simulation space is treated and what kind of results are desired. Another drawback of the FDTD method is the requirement of uniform meshing throughout the entire simulation space. This further increases the computational resource drain, as the mesh cannot be optimized to treat local regions of different characteristics more efficiently. Analogously, complete and uniform discretization of the temporal domain is required as well. Obtaining a certain time evolution in the simulation thus requires iteration to solve sequentially at each discrete time point, even if the value at a given point is not of interest. To further compound the added computational complexity due to this time discretization, there exists a condition to maintain stability of the method. This is known as the Courant-Friedrichs-Lewy (CFL) stability condition and it can be interpreted as an upper bound on the maximum time step, or distance between discrete time points of the simulation. This stability condition is given by (2-4a) for a general three dimensional space with unit cell dimensions $\Delta x \times \Delta y \times \Delta z$ and by (2-4b) for a one, two, or three dimensional space with cubic unit cells of side length $\Delta x$. In these equation $c$ is the speed of light in a vacuum.

$$\Delta t \leq \frac{1}{c}\left(\left(\frac{1}{\Delta x}\right)^2 + \left(\frac{1}{\Delta y}\right)^2 + \left(\frac{1}{\Delta z}\right)^2\right)^{-1/2} \tag{2-4a}$$

$$\Delta t \leq \frac{\Delta x}{c\sqrt{dimensions}} \tag{2-4b}$$

The CFL condition essentially sets a lower limit on the number of time iterations that must be solved to obtain a solution. Surpassing this limit will cause spurious exponential growth in field values that quickly destroys any useful results.

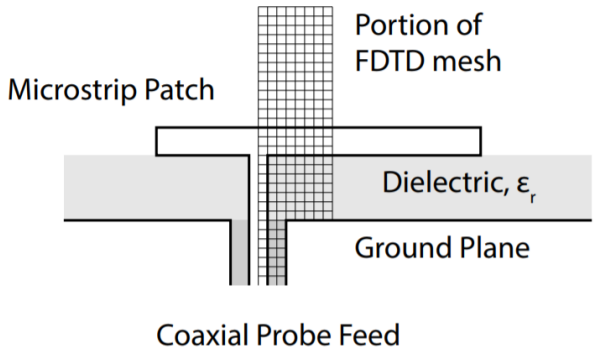


Figure 2.3: Meshing for microstrip patch antenna simulation.

All the discussed limitations are intimately related with regards to the challenge of applying the FDTD method to multi-scale problems. A uniform spatial discretization results in unnecessarily inflated usage of computational resources as regions of large feature size will have the same discretization resolution as regions of small feature size. Each additional discretization point requires memory to store as well as computation to solve for. Contributing to the same issue is the requirement that the entire simulation space be discretized. If a structure is simulated in free space for example, the free space region must be discretized at the resolution of the smallest feature and the field values at every point solved for regardless of whether they are relevant to the solution of interest. The time discretization requirement along with the maximum time step limit come into play in further increasing the amount of computation. From (2-4a), a finer spatial discretization will result in a larger maximum time step. Consequently, the small features of a multi-scale simulation will greatly increase the number of time iterations that must be solved to reach some desired time evolution. In the best case scenario, the multi-scale

problem becomes very computationally expensive perhaps requiring hardware upgrades of the computing platform for faster processing or more memory, and in the worst case scenario, the simulation simply becomes unreasonable to run.

## 2.2 Developments for Multi-Scale Simulations

With multi-scale electromagnetic problems having long existed, there have of course been attempts to overcome the discussed issues via extensions of the conventional FDTD method. Unconditionally stable methods, contour path models, non-uniform grids, and unstructured grids will be briefly summarized as some of the more well-established of such extensions. It will be demonstrated that while they do have their own advantages in certain application spaces, they ultimately do not address all the issues associated with performing general multi-scale simulations.

### 2.2.1 Unconditionally Stable Methods

Unconditionally stable FDTD methods attempt to modify the conventional method such that the CFL limit on the maximum time step no longer applies. Any size time step may thus be chosen without rendering the simulation unstable, allowing for a reduction in the number of time iterations that need to be solved. Unconditionally stable methods represent a rather large category and include the alternating direction implicit method [11], the Crank Nicolson method [12], and the locally one dimensional method [13], among many others. With regards to application for multi-scale problems, while the large number of time iterations due to resolution of fine features is overcome, the excessive memory usage is still present as the entire simulation space must still be meshed uniformly. Aside from not addressing this limitation, unconditionally

stable methods additionally take away certain advantages of the conventional FDTD method. Most notably, the explicit nature of the method is typically lost. Matrix inversion and the complications that come with it such, as sparse matrices or ill conditioned matrices, must be introduced. Finally, while it is true that the time step may be chosen arbitrarily without instability, practically there are still limits due to the numerical dispersion typically increasing with the timestep [14].

### 2.2.2 Contour Path Models

Another means of extending the conventional FDTD method to treat multi-scale problems is to use contour path models. These models are based on the concept of maintaining relatively larger unit cells as compared to those that would be required to rigorously resolve the fine features [4]. The effect of the fine features now occurring on a sub-cellular level is then accounted for indirectly by altering how the field values of the larger cells adjacent to the features are computed. Different models correspond to different means of altering the field values and depend on the fine feature being resolved, though they all have the similar characteristic of being derived from the contour integral form of Maxwell's curl equations, hence the name "contour path models". Figure 2.4 gives an example of modeling a thin sub-cellular material sheet. For the purposes of visualization, a two dimensional cross section of three dimensional space is shown. In this case the electric field $E_y$ of the unit cells which contain the sheet is split into $E_{y,out}$ and $E_{y,in}$ outside and inside the material respectively to account for discontinuity at the material interface when formulating the integral expressions. In contrast to the conventional method of directly using an appropriately small unit cell to resolve the fine features, such models allow for improvements in both memory and computation requirements.

At first glance, this seems to solve the issues associated with performing FDTD multi-scale simulations; however, the derivation of these models introduces other issues. Again, while the conventional FDTD algorithm is derived from the differential form of Maxwell's curl equations, these models are derived from the contour integral form. With general physical phenomena most often described in differential form, this shift to working with integral equations makes the creation of models that incorporate additional phenomena less straightforward. Thus, despite success of the contour path approach in modeling features such as thin slots [15], thin wires [16], material films [17], and many more, it is not appropriate for more general multi-scale problems.

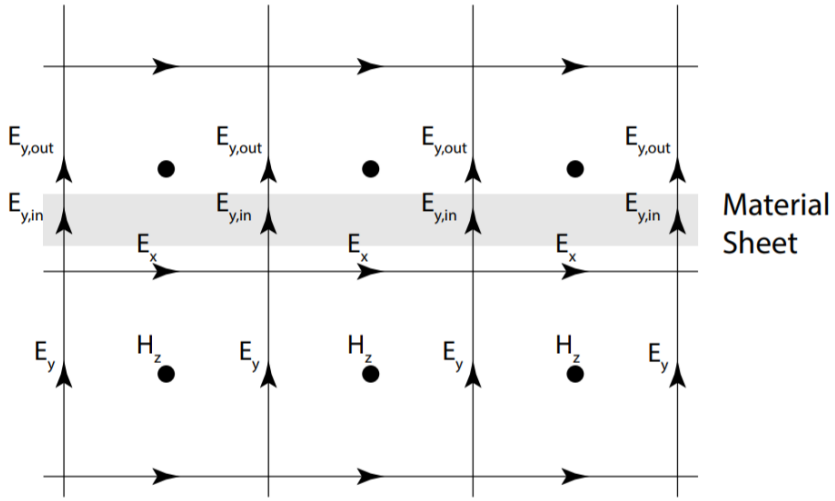


Figure 2.4: Contour path modeling of thin material sheet.

### 2.2.3 Non-Uniform and Unstructured Grids

While unconditionally stable methods overcome the excessive computation associated with having small unit cells and contour path models overcome the necessity to use small unit cells, probably the most intuitive means of approaching the multi-scale problem would be to modify the conventional FDTD algorithm such that uniform discretization is no longer needed. This would allow for the mesh to be optimized in terms of the system being modeled. This has

been accomplished through extensions that allow for non-uniform grids or unstructured grids. The difference between the two is that non-uniform grids allow for different sizes of orthogonal unit cells to be used in a single simulation [18] whereas unstructured grids allow for any configuration of arbitrary polyhedral cells [19]. In both cases the cells must still share common faces and edges. These grids seem to be quite attractive for use with multi-scale problems. Along with the reduction in memory requirements attributed from the fact that fine discretization may be used to represent small features whereas large discretization can be used for larger features, these grids also provide for a higher accuracy as compared to the contour path models [4]. Nevertheless, they are not appropriate for multi-scale simulations since the CFL limit remains. Consequently, the simulation time step is still limited by the smallest spatial dimension, and the number of time iterations that must be solved to reach a given time evolution is not increased from what it would have been using the conventional FDTD method. On top of this, the algorithm to implement these grids is derived from the integral form of Maxwell's curl equations which inhibits incorporation of additional phenomena as discussed previously. Unstructured

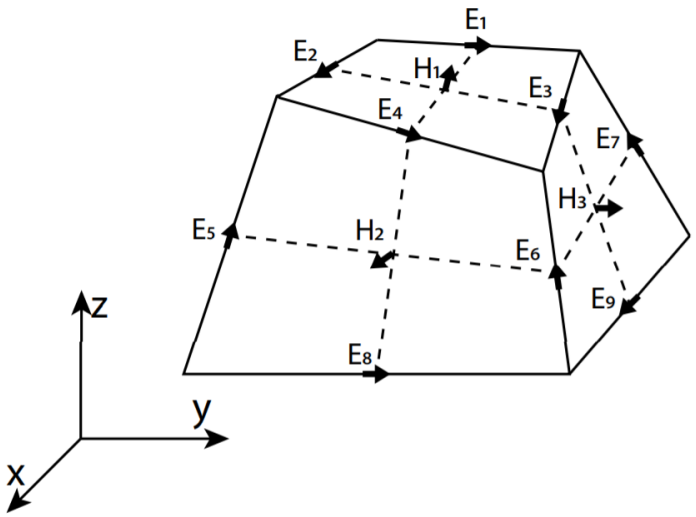


Figure 2.5: Unstructured grid cell.

grids have also been attempted by hybridizing the FDTD method and the finite element method [52], taking advantage of the fact that the finite element method inherently does not require structured meshing. However, the incorporation of a new computational method results in a loss of many of the advantages of the FDTD method discussed previously. A possible unstructured grid cell is visualized in Figure 2.5. These grids ultimately are suited more so towards conventional electromagnetic problems with geometries that cannot be accurately modeled using uniform orthogonal unit cells rather than multi-physics, multi-scale problems.

## 2.3 Developments in Sub-Gridding

### 2.3.1 Overview of Sub-Gridding

One extension of the conventional FDTD method that was omitted previously for the sake of dedicating an individual section to it is sub-gridding methods. Sub-gridding refers to the procedure of embedding local regions of small orthogonal unit cells into a base simulation mesh of relatively larger orthogonal unit cells [22], as shown in Figure 2.6 in two dimensions. While seemingly similar in concept to non-uniform gridding, sub-gridding does not require cells to share faces and edges meaning the fine discretization region may be better localized. The more significant difference between this method and the previous ones discussed however is the fact that it mitigates the limitations of conventional FDTD towards being applied to multi-scale problems without inherently removing any of its advantages. Not only are memory requirements reduced by allowing for different sizes of unit cells in a single simulation, but also computational requirements are reduced by allowing for local time steps in regions of differently sized cells. The maximum time step in the base mesh is thus ideally unaffected by the incorporation of any embedded meshes. On top of this, the field values in both fine and coarse discretization regions

are solved using the conventional differential equation based FDTD algorithm. The only modification to the algorithm is an introduction of a means to couple the regions. Sub-gridding consequently shows promise in being an appropriate extension of conventional FDTD to handle general multi-scale problems efficiently.

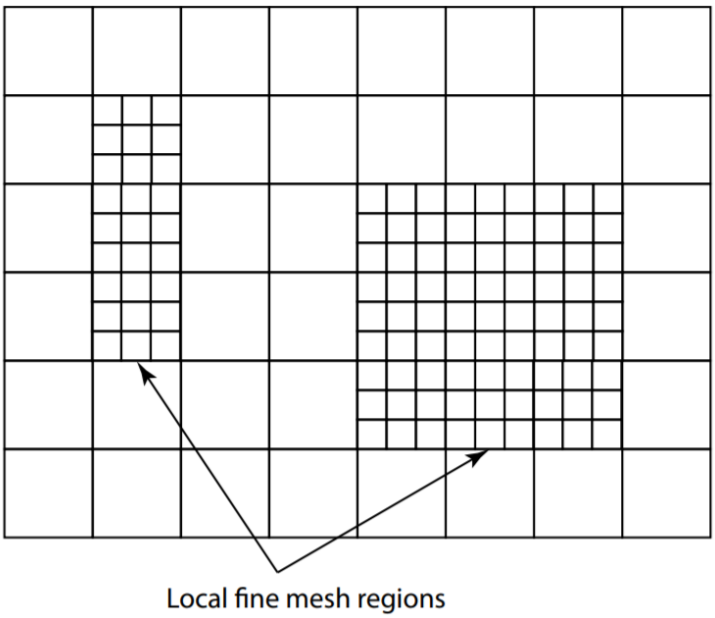


Figure 2.6: Sub-gridding mesh.

### 2.3.2 Past Developments

The concept of sub-gridding for the FDTD method had its origins in the "Expansion Technique" [20] where two separate conventional FDTD simulations were performed sequentially. The first simulation modeled the system on a large scale whereas the second modeled a local portion of the system containing fine details. Spatial and temporal interpolation of fields solved during the first simulation are used to obtain the fields on the simulation space boundary for the second simulation in order to couple the first simulation to the second. This work went rather unnoticed for some time until the 1990s where the number of publications

addressing the coupling of FDTD meshes of different spatial scales began to grow immensely. Rather than performing two separate simulations, [21] attempted to run a single simulation in which the simulation domain involved regions of both coarse and fine meshes. This would allow for coupling from both coarse to fine mesh as well as fine to coarse mesh simultaneously. The term "sub-gridding" was first used to describe such a concept in [22].

Initial means of sub-gridding more or less took the same approach. They all involved some general means of spatial and temporal interpolation in order to couple fields into the fine mesh region followed by some means of coarse mesh field correction using fine mesh fields to couple into the coarse mesh region. Interpolation based on a finite difference approximation to the second order wave equation was introduced in [22], efficiency was improved in [23], and the method was extended to three dimensions in [28]. Interpolation and correction based on an integral approach known as the finite integration technique was formulated in [24], a method involving time extrapolation and spline interpolation was used in [25], and a second order Taylor expansion based interpolation was used in [29].

An important factor in making sub-gridding useful for general problems is the support for material traverse where simulation structures may cross through the coarse-fine mesh interface. The interpolation treatment in [26] allowed for both dielectric and perfect electric conductor (PEC) traverse of the interface. A current based method of coupling the fine and coarse meshes that also allowed for traverse of dielectrics and PECs was introduced in [31].

Many of the methods to follow were quite similar to those that came before them with some minor adjustments [32, 35, 43, 47, 49]. Some of the more novel ideas however include coupling of the fine and coarse regions using the surface equivalence theorem [36, 41], coupling using finite element inspired concepts [38], and separated interfaces for temporal and spatial sub-

gridding [40]. These sub-gridding methods have additionally inspired hybrid methods as well such as in [34] where the alternating direction implicit method is incorporated, [37] where the finite element method is incorporated, [45] where a model order reduction method is incorporated, or [46] where higher order FDTD is incorporated.

A big problem with modifications to the FDTD method in general is that stability is often difficult to guarantee. Sub-gridding methods are no exception, and it is well known that most implementations suffer from what is often called “late time instability”. This type of instability has the distinguishing characteristic that it is not detectable until a large number of time iterations have been performed. The origins of late time instability are not clear due to the fact that it has been notoriously difficult to derive analytic stability conditions for sub-gridding methods [48]; however, a number of publications have attempted to tackle this problem. In [24, 39, 40], the sub-gridding algorithm proposed was formulated as a set of matrix equations. While an explicit stability condition could not be developed, general guidelines in terms of properties of the matrices in terms of symmetry or being positive definite were derived. Maintaining these properties allows for guaranteed stability for some undetermined time step. In [27, 30], an interpretation of the sub-gridded FDTD algorithm using dual circuit equations was developed. It was postulated that in order to maintain stability of the algorithm, the dual circuit had to involve solely passive components. In [33], it was proposed that the source of late time instability is the differences in group velocity in the coarse and fine meshes. Spatial filtering was performed in order to ensure that only fields with wavenumbers such that the group velocity in each mesh was approximately the same remained to enhance stability. Spatial filtering for stability purposes with sub-gridding was performed again in [44], but not with the group velocity interpretation of instability, but rather with the CFL interpretation. In [38], finite element concepts were applied

to allow for stable coupling of meshes. Most recently, [48, 50] formulated the FDTD method in the form of a dynamical system. Conditions were then derived to ensure that such a system remained dissipative, allowing it to remain stable.

### 2.3.3 Issues in Applicability

From the previous section, it is clear that there has been, and still continues to be, extensive research on developing sub-gridded FDTD. Despite these developments, an accepted general sub-gridded FDTD method does not exist either in the academic community or in industry. The reasons for this have been hinted at in the previous section and will be explicitly discussed in detail here. Specifically, all previously developed sub-gridding methods have been lacking in a combination of stability, material traverse, and efficiency.

The necessity of stability in a numerical method is obvious; without it, simulation results would be unphysical and useless. Unfortunately, late time instability is ubiquitous in nearly all sub-gridding algorithms. Reiterating from the previous section, this is a category of instability whose effects are not evident until a large number of time iterations have been solved. An example of a time domain field waveform of a simulation demonstrating late time instability is shown in Figure 2.7. It may be observed that in the early time iterations there is no detectable sign of instability. This characteristic of late time instability has introduced a gray area in terms of acceptability. In the time iterations prior to the emergence of this instability, fidelity of the simulation results is maintained; thus, some argue that late time instability is not a problem so long as it occurs after a large enough time iteration that practical simulations would not be affected. Often, researchers will even reduce generality of their algorithms by introducing empirical field averaging [25] or increase computational efficiency by spatial filtering [44] in

attempts to delay the onset of this late time instability. However, late time instability has another characteristic that is frequently overlooked—its obscurity. The inability to analytically describe this instability leads to a lack of understanding not only about its origin but also about its onset and how to prolong it. Though many researchers use methods that successfully suppress this instability in a specific scenario, its onset in general problems is extremely unpredictable [28], making algorithms that possess it unusable for the most part. There are few publications that attempt to present a sub-gridding algorithm that is stable by construction rather than simply one with a suppressed instability; these publications are mentioned in the previous section. Nevertheless, all of these are still plagued by other problems that prevent general applicability.

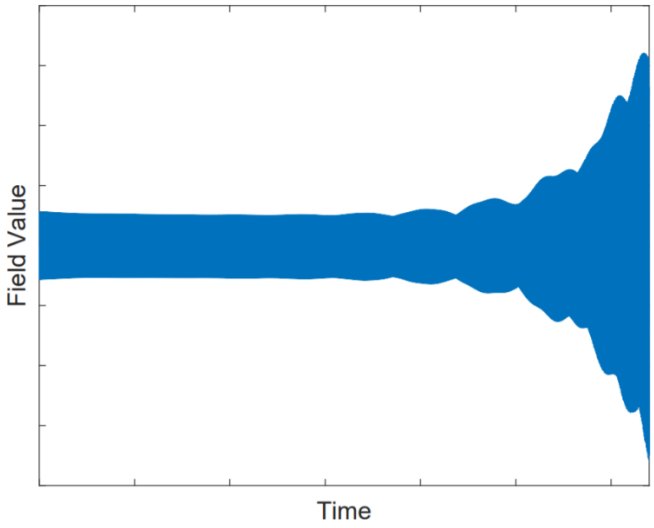


Figure 2.7: Late time instability.

One of these other problems is material traverse. Support for material traverse in a sub-gridding algorithm is another necessary characteristic to allow general applicability and thus widespread acceptance. As briefly mentioned earlier, material traverse refers to the situation in which the fine-coarse interface is not fully located in a region of constant material properties. Support for this scenario allows for materials to extend from one mesh to the other across the

interface, as shown in Figure 2.8. Clearly, in a multi-scale simulation the features that are desired to be discretized at a finer resolution are not in general suspended in a region of homogeneous material such that a fine-coarse interface is fully located in a single material. A fair number of methods proposed in past literature have attempted to treat this problem as mentioned in the previous section. Among those that also have some degree of provable stability are [24, 39, 48]. Between these, [24] and [39] can handle only PEC traverse whereas [48] can handle dielectric and conductors but not PEC traverse. Yet even neglecting the issue of limited material traverse support, these algorithms are not acceptable for general use due to one more reason.

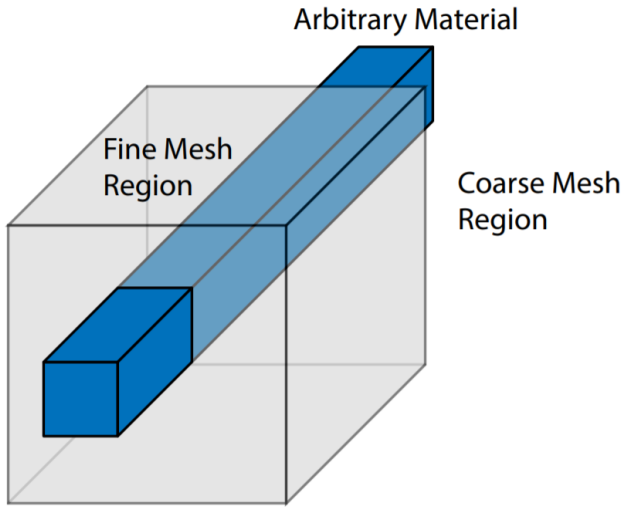


Figure 2.8: Material traverse.

Neglecting material traverse capabilities for the time being and considering all the sub-gridding methods claiming to be stable by construction, there is also the problem of efficiency. As discussed previously, one of the most attractive features of sub-gridding is that it allows for local time steps. Thus, in accordance with the CFL limit, while the fine mesh would require a small time step due to its fine resolution, the coarse mesh may use a larger one due to its larger

spatial resolution. This improves efficiency as the number of computations required to achieve some final time evolution of the system is greatly reduced. In fact, this improvement in efficiency is one of the biggest factors separating sub-gridding methods from non-uniform grid or unstructured grid methods. Unfortunately however, none of the methods that are stable by construction have been able to realize this efficiency benefit. In [24, 39, 40] using the matrix form approach to have stability by construction, stable simulations either reported a time step that had to be reduced to that for which efficiency improvements were nonexistent, or the time step was not mentioned at all. In such cases where the time step was not mentioned explicitly, it is assumed that the same efficiency issues were experienced. In [38, 48, 50] which use various other methods to propose a stable sub-gridded method by construction, a global time step was assumed from the very beginning, thus efficiency benefits were never expected.

# CHAPTER 3

# A General Sub-Gridding Method

## 3.1 Preliminary Information

The new proposed means of sub-gridding spawned from a collective analysis of past literature as well as persisting issues in realization. Prior to delving into the implementation and details of the method however, the establishment of some preliminary information is in order. This information will facilitate understanding of key aspects of the algorithm as well as any accompanying figures.

### 3.1.1 Spatial Domain

For the proposed method, just as with sub-gridding methods in past literature, integration of the fine mesh locally into the coarse mesh is accomplished by directly replacing coarse mesh cells with fine mesh ones. In other words, the cells of each mesh do not share edges or faces and there is no structural change leading to non-uniformity or non-orthogonality existing in any individual region. In all subsequent figures and explanations, a unit cell with electric field edge components will be assumed as in Figure 2.1. Consequently, located on the interface between the fine and coarse mesh will be tangential electric field components and normal magnetic field components. A two dimensional visualization of a portion of the three dimensional interface is provided in Figure 3.1. For the remainder of this thesis, two dimensional visualizations of three dimensional FDTD meshes will be used primarily. Additionally, for the purpose of distinguishing between the two meshes, electromagnetic fields of the coarse mesh will be

denoted with upper case letters whereas fields of the fine mesh will be denoted with lower case letters. Specific components will be referenced using lower case letter subscripts. Subsequent explanations will additionally assume an odd refinement factor as in general, this allows for collocation of coarse and fine mesh interface field components and leads to a simpler algorithm. With this being said, there is nothing inherent about the algorithm that poses a barrier to

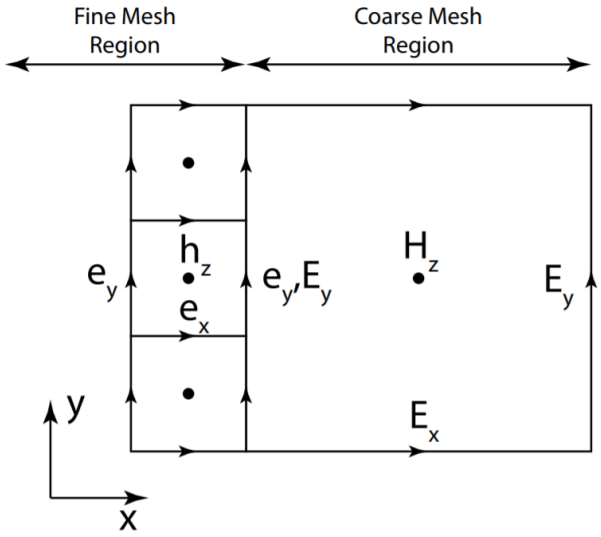


Figure 3.1: Spatial domain of proposed method.

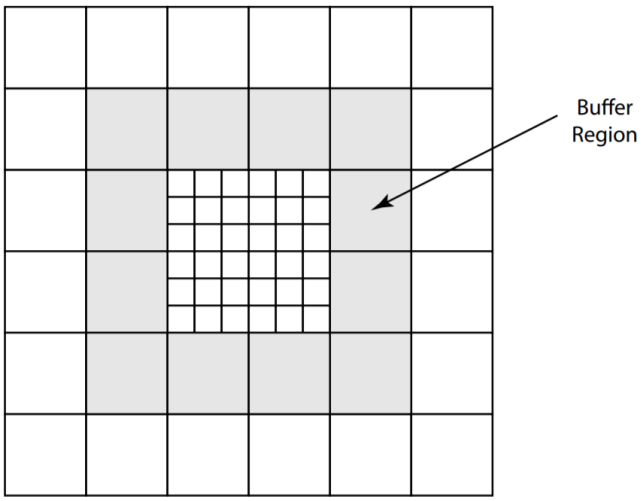


Figure 3.2: Buffer region.

treatment of even refinements. Figures will specifically demonstrate the case of an odd refinement of three. Finally, the region corresponding to the coarse mesh unit cells located immediately adjacent to the coarse-fine interface will be referred to as the “buffer region”. This region is indicated as the shaded area in Figure 3.2 and is important in the coupling of fine and coarse regions as will be evident later.

### 3.1.2 Temporal Domain

Based on the CFL limit, the ratio of the maximum time step in the coarse mesh to that of the fine mesh must be equivalent to the spatial refinement factor. Thus, for the proposed method the time steps used in each mesh, whether chosen to be at the maximum or not, will have a ratio equal to the spatial refinement. In other words, the number of time iterations that must be performed in the fine mesh to have the same total time evolution as one time iteration of the coarse mesh is equal to the refinement. To reiterate, the subsequent algorithm overview will assume an odd refinement and the subsequent figures will assume a specific odd refinement of three. With the fine mesh fields essentially having a higher sampling frequency and being solved at more discrete time points as compared to the coarse mesh fields, it is chosen to have alignment of the electric field samples of each mesh in time as shown in Figure 3.3. This figure visualizes the temporal locations at which all the fields are solved and it may be seen that for an odd refinement, in aligning the electric field samples, the magnetic field samples will also turn out to

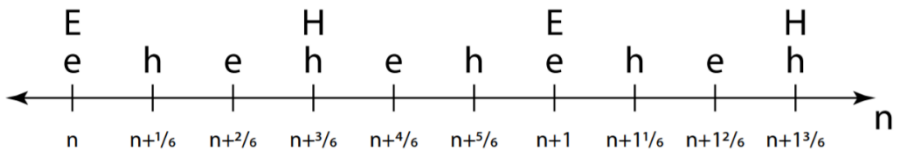


Figure 3.3: Time locations of solved fields in the proposed method.

be aligned. Ultimately however, this behavior is irrelevant to implementation of the algorithm.

### 3.1.3 Known Fields

In performing any FDTD based simulation, there must be some arrangement of known field values in time at the beginning of each time iteration. Solving to move on to the next time iteration causes a uniform shift in all these known values forward one time step, thus their arrangement with respect to one another remains unchanged. For the proposed method, this arrangement of known fields relative to one another is indicated in Figure 3.4. All components for a given field are assumed to be known at their respective time location for all discretized spatial locations. After solving a time iteration to evolve one coarse mesh time step forward, the relative locations of the known values in time remains the same. One important thing to recognize here is that for a given initially known field value, it is inherently implied that all values occurring at past times are also known. Clearly, simulating up to some point in time then values from the beginning of the simulation up to that point should have been solved for and thus known; however, values at times prior to the start of the simulation are also taken to be known. No generality is lost with such an assumption as the vast majority of time domain electromagnetic simulations assume zero initial dynamic field everywhere in space. Field values are thus known for all times prior to any excitation, with spatial distributions typically chosen as part of the simulation setup.

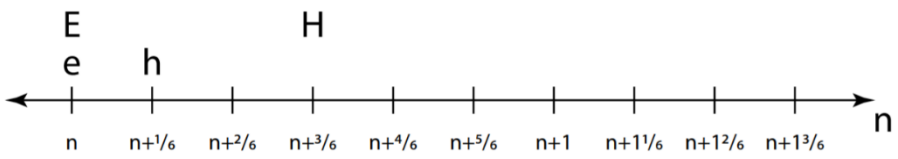


Figure 3.4: Initially known fields at the start of a time iteration.

## 3.2 Overview of the Algorithm

With the preliminary information taken care of, the proposed sub-gridding method can now be examined in greater depth. The steps of implementation will be enumerated followed by a detailed discussion of certain aspects of the method. This section then concludes with an analysis of how the issues in realization that have plagued past methods were treated.

### 3.2.1 Steps of Implementation

1) Magnetic field components in the coarse region are interpolated in time using the known value at both the current and previous timestep to obtain values at the currently known time location of the magnetic field components in the fine mesh region. This interpolation is described by (3-1) and visualized in Figure 3.5.

$$H_{int} = \frac{1}{refinement}\left( H|^{n-1/2}\left(\frac{refinement-1}{2}\right) + H|^{n+1/2}\left(\frac{refinement+1}{2}\right)\right) \quad (3\text{-}1)$$

This time interpolated magnetic field will be referred to as $H_{int}$. Following this interpolation, all the coarse mesh electric and magnetic field components are known at the same time locations as their corresponding fine mesh fields.

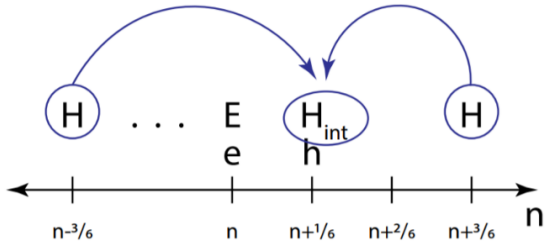


Figure 3.5: Time interpolation in step 1.

2) The necessary coarse and fine mesh electric fields as well as the necessary time interpolated

magnetic fields and fine mesh magnetic fields are used to spatially interpolate for electric and magnetic fields at locations within the buffer region. Trilinear interpolation is applied for most of the results later presented in Chapter 4. This interpolation method is described by (3-2) to obtain the value at a point within the general mesh cell shown in Figure 3.6.

$$k(x,y,z) = \frac{1}{\Delta x \Delta y \Delta z}\begin{bmatrix}(\Delta y - y) & y\end{bmatrix}\begin{bmatrix}(\Delta x - x) & x & 0 & 0\\ 0 & 0 & (\Delta x - x) & x\end{bmatrix}\begin{bmatrix}k_{111} & k_{112}\\ k_{211} & k_{212}\\ k_{121} & k_{122}\\ k_{221} & k_{222}\end{bmatrix}\begin{bmatrix}(\Delta z - z)\\ z\end{bmatrix} \qquad (3\text{-}2)$$

In this case *k* represents either an electric or magnetic field component in space, and the equation assumes $k_{111}$ to be the origin for the sake of simplicity.

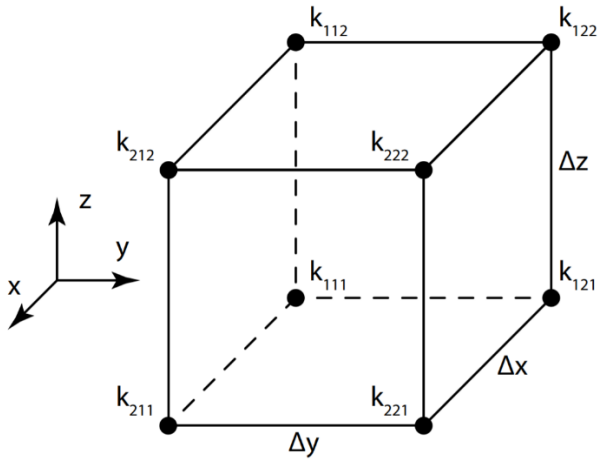


Figure 3.6: Trilinear interpolation points.

The locations of interpolated fields within the buffer region correspond to the spatial locations that would exist assuming the buffer region is composed of fine cells. In other words, after this interpolation it may essentially be interpreted that the fine mesh region has been extended into the buffer region. This combination of the fine mesh region with the spatially interpolated field values in the buffer region will be referred to as the "extended fine mesh region". Figure 3.7 visualizes the extended fine mesh region as well as indicates in gray the effective fine cells of the

buffer region. Figure 3.8 visualizes the known fields following the completion of this step, where $e_{ext}$ and $h_{ext}$ represent the fields within the extended fine mesh region.

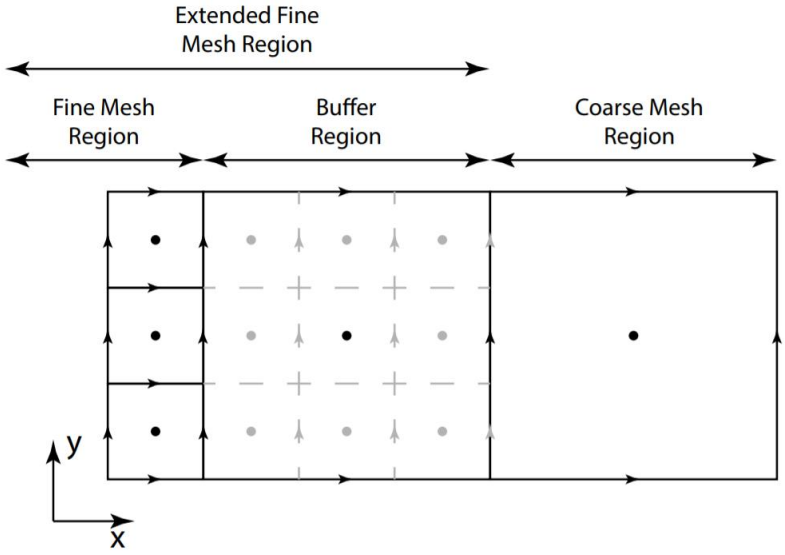


Figure 3.7: Spatially interpolated fields in buffer region.

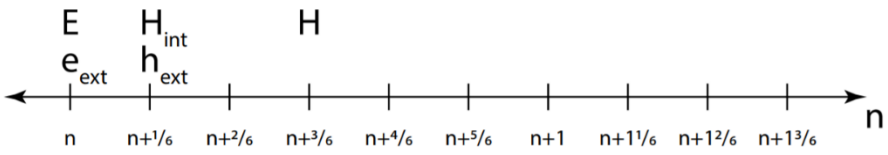


Figure 3.8: Known fields after step 2.

3) Conventional FDTD is performed in the extended fine mesh region for a number of time iterations equal to the refinement. The known fields following the completion of all these time iterations are visualized in Figure 3.9.

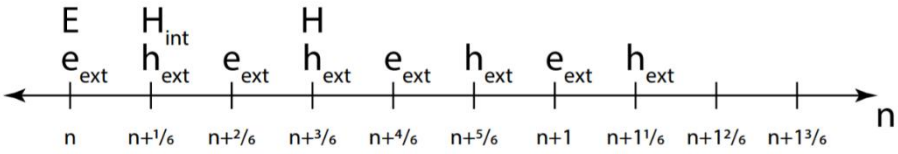


Figure 3.9: Known fields after step 3.

4) The field values of the buffer region are discarded as they are no longer of use. Figure 3.10 visualizes the known fields after this step where the ‘ext’ subscripts have been dropped to represent the buffer region fields being discarded.

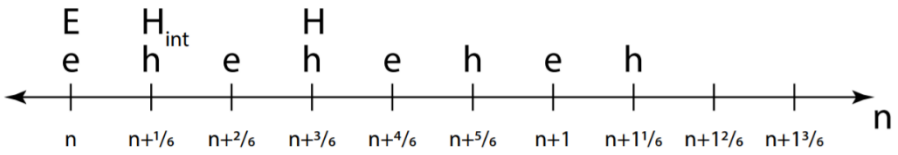


Figure 3.10: Known fields after step 4.

5) From here, the fine mesh electric field components collocated with those of the coarse mesh on the coarse-fine interface are seen to be exactly those coarse mesh values at the next timestep of the coarse mesh. The collocated interface coarse mesh electric fields are thus set to be equal to these fine mesh values. All other coarse mesh electric field values not located on the coarse-fine interface may then be solved for the next time step using the conventional FDTD algorithm. All coarse mesh magnetic field values can subsequently be solved for next time step likewise using the conventional FDTD algorithm. From Figure 3.11 it may be seen that the known field values have all evolved one coarse mesh time step from those initially known throughout all space. Consequently, the time iteration is complete.

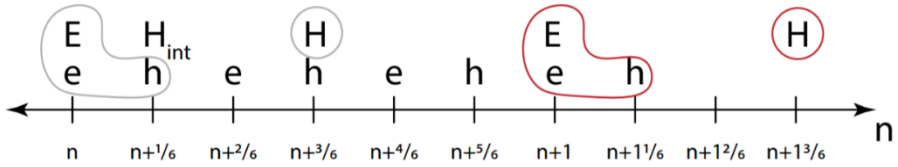


Figure 3.11: Known fields after step 5.

6) Repeat steps 1-5 to continue solving for future times.

### 3.2.2 Discussion of Implementation

With the steps to implement the algorithm laid out above, there are some details that are worth expanding upon to better appreciate how the proposed method works. With sub-gridding, the principal problem is how to treat the coarse-fine interface. This interface is not only where information is transferred back and forth between the fine mesh and the coarse mesh, but also it is where the conventional FDTD algorithm can no longer be applied. Specifically, it may be seen that on this interface and with the assumed known field values at the beginning of the time iteration there is no means of solving for the tangential electric fields at the next time step in either the fine or coarse meshes. This interface is the simulation space boundary of the coarse and fine mesh regions. Conventionally, simulation space boundaries can be defined to be either perfect electric conductors or perfect magnetic conductors. Alternatively, a boundary condition which absorbs incident fields may be implemented depending on the type of simulation being performed. Clearly, none of these are appropriate for this coarse-fine interface and some other treatment must be applied to obtain the boundary values and allow for FDTD simulation to proceed in each simulation space. Based on the arrangement of known field values at the beginning of the time iteration, in the coarse mesh region all electric field values can be solved for the next time step by conventional means except for the tangential components lying on the coarse-fine interface. Once these are found, all the coarse mesh magnetic field values can be solved to complete one time iteration in the coarse mesh. A similar issue exists in the fine mesh; however, due to the fact that a number of fine mesh time iterations equal to the refinement is required to evolve the fine mesh fields one coarse mesh time step, the problem becomes much more complicated. Values of tangential electric fields on the interface must be found now for multiple time instances instead of just one for a given coarse mesh time iteration. Finally, the

interface electric field values in both the coarse and fine regions must be ultimately be such that information may be transferred between the regions. All of these problems are treated using the concepts of the buffer and extended fine mesh regions.

Fields in the buffer region are obtained by first performing a time interpolation of coarse mesh magnetic fields to obtain values at the same timestep as the known fine mesh magnetic fields. This time interpolation is required in order to have accurate subsequent spatial interpolation that uses field values all at the same time location. No time interpolation for electric field in the coarse region is necessary as there is time alignment assumed. Spatial interpolation is then performed to obtain electric and magnetic field values in the buffer region such that it can be combined with the fine mesh region to create the extended fine mesh region. Given that areas outside of the original fine mesh region should not need high spatial resolution to accurately model the field distribution or simulation structure, this spatial interpolation is justified in terms of accuracy. From here, conventional FDTD is performed in the extended fine mesh region a number of time iterations equal to the refinement. While there still exists the issue of unknown boundary field values in this extended region, the boundary has been extended beyond that of the original fine mesh region. Consequently, in a refinement number of timesteps the error due to whatever erroneous value the boundary fields may have will not affect the original fine mesh region. This is visualized in Figure 3.12 for an assumed refinement of three. The field components labeled in red indicate erroneous field values resulting from unknown boundary fields. It may be seen that though the error propagates as time iterations are solved, it will not affect the interface electric fields when a refinement number of time steps are solved. The values in the buffer region, on the other hand, will have been corrupted and are thus discarded accordingly. The fields in the original fine mesh region have now been time evolved one coarse

mesh time step. Additionally, the interface coarse mesh electric field values at the next timestep are exactly the new collocated fine mesh electric field values. Conventional FDTD can then be used to obtain the rest of the fields at the next time step in the coarse mesh and complete the coarse mesh time iteration.

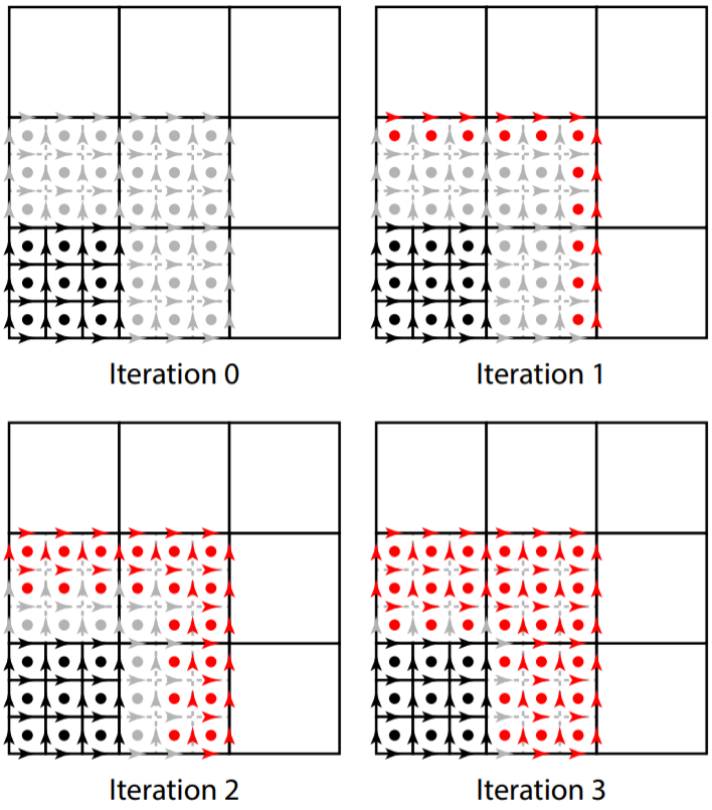


Figure 3.12: Corrupted fields on each time iteration.

## 3.3 Treatment of Issues in Applicability

The issues in applicability of past sub-gridding methods were stated to be stability, material traverse, and efficiency. In stability and efficiency, there is no direct treatment as of yet. Clearly, the algorithm is derived for the case of both co-located temporal and spatial sub-gridding interfaces as well as local time steps in the coarse and fine meshes for maximum efficiency, but the lack of a formal stability analysis makes the benefit of these traits somewhat

hollow at this point. As with other sub-gridding methods that have stability analyses associated with them, ensuring stability may require reduction of efficiency, but this is unknown at this time. Nevertheless, this method lends itself well to a stability analysis. Unlike other sub-gridding algorithms that rely on second order and higher interpolation schemes for their accuracy, this algorithm is already quite accurate using just linear interpolations. This supports the usage of linear algebra in order to perform a stability analysis and derive conditions for stability.

In terms of material traverse, the proposed algorithm is theoretically well suited to handle dielectric traverse inherently with minimal modifications to the algorithm. For a dielectric traverse across the coarse-fine interface, based on the principle of the algorithm it is known that so long as accurate field interpolation in the buffer region can be accomplished, there should be no issues in accuracy and validity of the algorithm. Magnetic field interpolation in the buffer region may be performed with no special treatment as magnetic fields are continuous across the interface of a dielectric. Interpolation of tangential electric field components may also be accomplished with issues following the same reasoning. The only potential problem lies with interpolation of normal electric fields across the interface where it is known that they are discontinuous. However, this can be easily treated by first converting these components to components of electric displacement as defined in (3-3), where $\varepsilon_r$ and $\varepsilon_o$ are the relative and free space permittivity respectively.

$$\vec{D} = \epsilon_r \epsilon_o \vec{E} \tag{3-3}$$

It is well known from electromagnetic theory [51] that the normal components of electric displacement are continuous across a dielectric interface so long as no free surface charges exist. Thus, interpolation can now be performed after which the electric displacements are converted

back to electric fields. The conversion procedure prior to interpolation is visualized in Figure 3.13.

Overall, the promise of this proposed method lies in the fact that it is different in approach as compared to methods of the past. It does not obtain the troublesome interface fields directly from interpolation or extrapolation or integral methods or equivalent source methods. Rather, it obtains then from the conventional FDTD algorithm itself. The consequences of such an approach are still in need of further analysis.

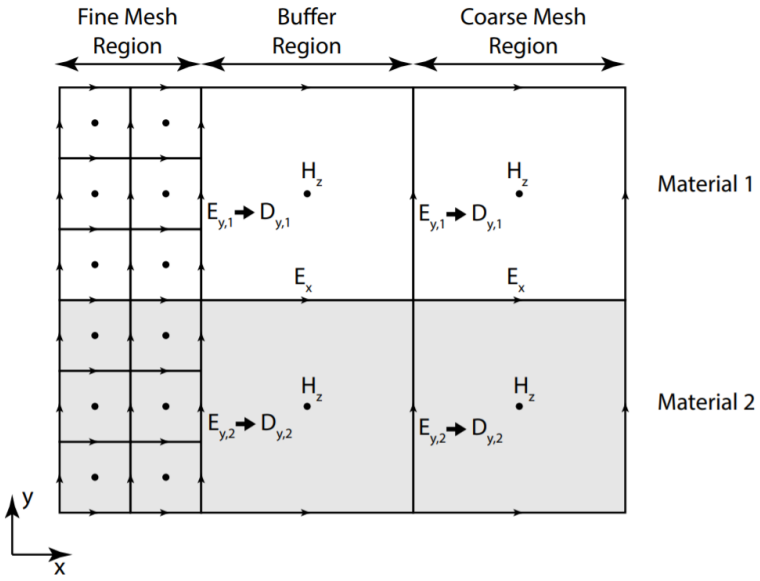


Figure 3.13: Material traverse with the proposed method.

# CHAPTER 4

# Numerical Results

Various numerical tests were performed to assess the capabilities and characteristics of the proposed sub-gridding method. Among those discussed in this chapter include the simulation of an electric line source radiating in the presence of a conducting sphere. Results are compared with those found using the conventional FDTD method for the purposes of verification as well as investigation into the practicality of sub-gridding. A direct test of numerical reflection from the coarse-fine interface is also performed. Several parameters are varied in this case to evaluate accuracy of the coupling between coarse and fine meshes and the factors that contribute to improving it. Finally, the proposed method is analyzed in the late time through the simulation of a resonant cavity. A large number of time iterations are solved in an attempt to reveal any intrinsic instabilities or other spurious behaviors.

## 4.1 Radiation in the Presence of a Conducting Sphere

### 4.1.1 Motivation

A good way to both verify that the proposed sub-gridding method in fact produces meaningful results as well as assess its application space is to directly compare it with the conventional FDTD method. After all, not only does the conventional method already have a well proven track record, but also the goal of the proposed method is ultimately to extend the range of applicability from that of the conventional method. With the specific application space of interest being multi-scale simulations, the comparison is made by simulating an electric line

source radiating in free space in the presence of a conducting sphere as shown in Figure 4.1. Such a scenario was chosen due to the fact that while a coarse mesh is sufficient to model the fields in free space where they will have relatively low spatial variation, a finer mesh is better able to model the sphere. It may be recalled that FDTD requires orthogonal rectangular cuboid unit cells and so curved surfaces are subject to a "staircase" approximation. With finer cells this approximation improves, allowing for more accurate modeling and thus more accurate results. A cross section of a sphere modeled using orthogonal cells is shown in Figure 4.2; as the cell size decreases the model is more accurate. Simulation is performed using each of a fully coarse mesh conventional FDTD method, a fully fine mesh conventional FDTD method, and the proposed sub-gridding method. The fully coarse mesh represents the case where the resolution is sufficient for fields in free space but crude in terms of modeling the sphere, whereas the fully fine mesh

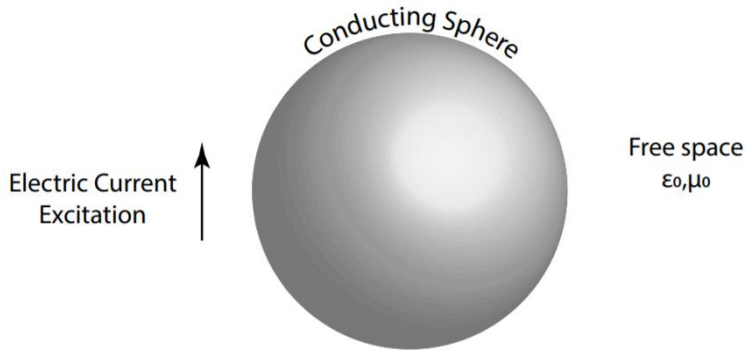


Figure 4.1: Radiation in the presence of conducting sphere simulation scenario.

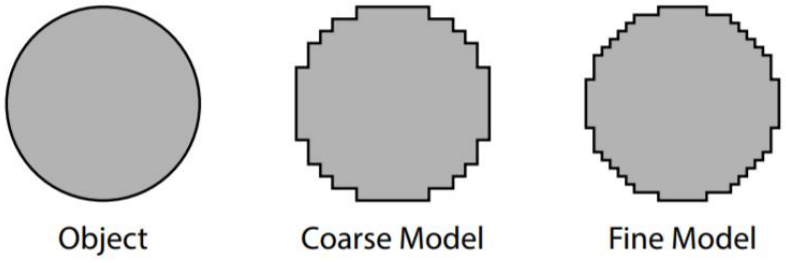


Figure 4.2: Staircasing approximation.

represents a more accurate modeling of the sphere. The sub-gridding is applied with fine and coarse meshes with the same resolution as the fully fine and fully coarse meshes respectively.

### 4.1.2 Simulation Setup

Going into the specifics of the scenario, the sphere is taken to have a diameter of 240 mm and a conductivity of 6e7 S/m. The electric line source is z directed, 75 mm long, and sinusoidally excited with a frequency of 1 GHz. In terms of location, the source is 105 mm away from the sphere and centered on an axis of symmetry of the sphere. The observation point at which fields are probed is located on the same axis, but on the opposite side of the sphere. This point is also 105 mm away from the sphere. Figure 4.3 illustrates some of these specifications as well as some characteristics of the simulation setup. Ultimately there were five separate simulations run for which results will be analyzed. One corresponds to a fully coarse mesh, two correspond to a fully fine mesh with refinements of three and five with respect to the fully coarse mesh, and two correspond to a sub-gridded mesh with similar refinements of three and five. For all simulations, the time step was chosen to be 0.99 of the maximum under the CFL limit. The fully coarse mesh used a simulation space composed of 60x60x60 cubic unit cells with the edge of a cell measuring 15 mm. The fully fine mesh used a simulation space of 140x140x140 and 220x220x220 cubic unit cells with cell edges of 5 mm and 3 mm for the cases of a refinement of three and five respectively. Finally, the sub-gridded simulation space was the same as that of the fully coarse mesh with the exception of an inclusion of a fine mesh region of dimensions 330x330x330 mm into the center. The unit cell size of this region is the same as that of the fully fine mesh for a given refinement. Linear interpolation was used in all sub-gridding cases to

determine the fields existing in the buffer region. Each simulation space included a ten cell thick perfectly matched layer to replicate the infinite extension of free space.

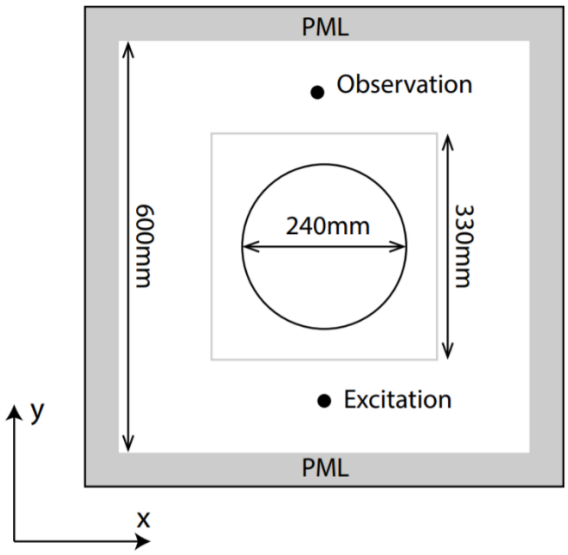


Figure 4.3: Schematic of simulation setup for radiation in the presence of conducting sphere.

### 4.1.3 Simulation Results

Time domain results for the case of a refinement of three are shown in Figure 4.4 for the z component of the electric field probed at the observation point. With a quick glance it may be seen qualitatively that the discrepancy between the sub-gridding results and the fully fine mesh results is much smaller than that between the fully coarse mesh and the fully fine mesh. The charts of Figure 4.5 quantify this error for each refinement case well as list the runtimes of every simulation and verify that significantly improved accuracy is achieved using the sub-gridded method as opposed to the fully coarse mesh. The percent errors as displayed in these charts are calculated (4-1), where $E_z$ refers to the z component of electric field for either the sub-gridded case or fully coarse mesh case and $E_{z,f}$ refers to that of the fully fine mesh case. The summation is over all time samples solved for in the simulation.

$$Percent\ error = 100 \cdot \frac{\sum_n \left| E_z(n\Delta t) - E_{z,f}(n\Delta t) \right|}{\sum_n \left| E_{z,f}(n\Delta t) \right|} \tag{4-1}$$

With regards to runtime, the fully coarse mesh had the shortest. This is to be expected given the relatively small number unknowns solved for on each time iteration as well as the small number of total iterations required to achieve a given time evolution of the system. The fully fine mesh had the longest runtime, again to be expected for analogous reasons. The runtime of the sub-gridded method was in between these two extremes but was nevertheless a substantial improvement over that of the fully fine mesh. For a refinement of three, the runtime of the sub-gridding method was approximately 13% that of the fully fine mesh, and for a refinement of five this number decreased to approximately 10%. This demonstrates the ability of the sub-gridding method to treat multi-scale problems in a more computationally efficient way than using a fully fine mesh.

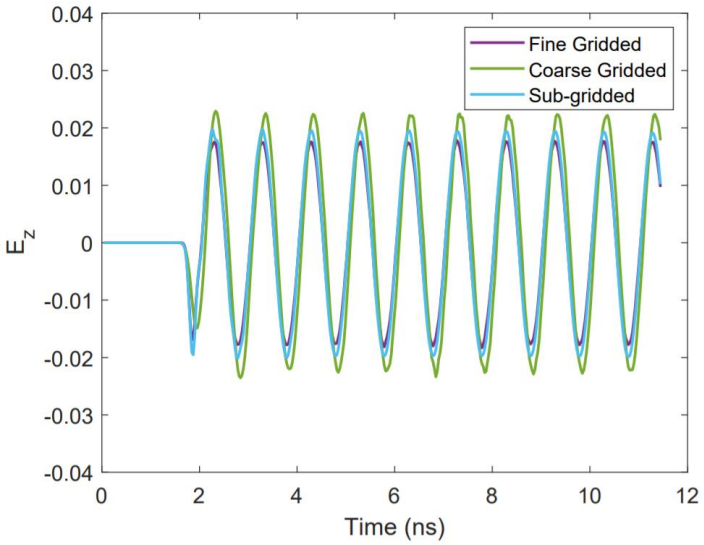


Figure 4.4: Probed field for refinement of three.

For the same simulations spatial domain plots are also generated along an observation line as shown in Figure 4.6 for various time instances. The intention of these plots is to demonstrate

| | Percent Error (%) | Runtime (sec) |
|---|---|---|
| Coarse Gridded | 46.9 | 43.0 |
| Sub-Gridded | 11.7 | 235.2 |
| Fine Gridded | — | 1,753.0 |

| | Percent Error (%) | Runtime (sec) |
|---|---|---|
| Coarse Gridded | 56.5 | 43.0 |
| Sub-Gridded | 24.7 | 1,221.5 |
| Fine Gridded | — | 12,084.7 |

Figure 4.5: Percent error and runtime for refinement of three (top) and five (bottom).

that the distribution of fields in general agrees better with the fully fine mesh case when using the sub-gridded method as opposed to a conventional filly coarse mesh. The results are shown for a refinement of three in Figure 4.7 for time instances of 4.27ns, 4.39ns, 4.50ns, 4.62ns, and 4.73ns corresponding to data points on a quarter wavelength of the fine mesh waveform going from peak to peak. Again, a qualitative examination shows that the spatial distribution of the z

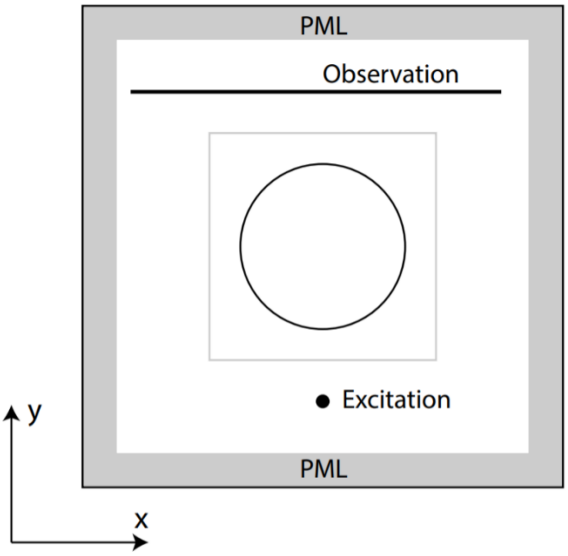


Figure 4.6: Observation line for spatial domain field plots.

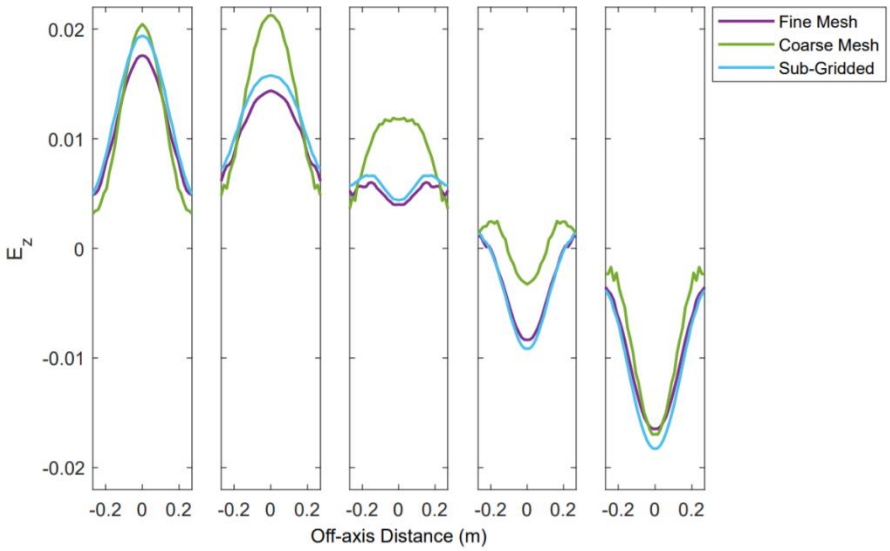


Figure 4.7: Spatial distribution of field for a refinement of three for various time instances.

component of the electric field are much improved using the proposed sub-gridding method as compared to using the conventional fully coarse mesh. Overall, this numerical test clearly shows the capabilities of the proposed method in increasing the accuracy of multi-scale simulations without suffering from the huge resource requirements of using a globally fine mesh.

## 4.2 Interface Reflection

### 4.2.1 Motivation

While the previous section demonstrated well the capabilities of the sub-gridding method in comparison to the conventional method for a specific simulation scenario, it is desired to have a more application-independent analysis. Results from such an analysis do a better job of generally characterizing the method. Following this motivation, reflection from the interface between the coarse mesh and fine mesh will be examined to quantify the quality of coupling between meshes. In theory if the coupling were perfect, a wave propagating from one region to

another would experience no reflection at the interface. On the opposite extreme if there were no coupling whatsoever, for example if the interface was a perfect electric conductor sheet, then there would be complete reflection. The amount of reflection is consequently one potential figure of merit to describe coupling between meshes.

### 4.2.2 Simulation Setup

To obtain the reflection information, the proposed sub-gridding method is applied to model a free space region where half of the space is discretized with a coarse mesh and the other half with a fine mesh. The FDTD total-field/scattered-field (TF/SF) technique is then implemented in which a numerical boundary is introduced in the simulation space. Within this boundary both the incident field from excitations and the scattered field from any reflections will exist whereas outside the boundary only the scattered field remains. The application of this technique is critical as it allows for scattered reflections from the coarse-fine interface to be accurately extracted. A sinusoidal plane wave is excited in the total field region of the coarse mesh traveling towards the coarse-fine interface. When this wave is incident on the interface there is some numerical reflection, which then propagates back through the total field region toward the TF/SF boundary. Once it reaches this boundary, the reflected wave alone is transmitted and may be used to determine the reflection coefficient of the interface. This simulation scenario is visualized in Figure 4.8 where an x-polarized z-directed plane wave is assumed. The superscripts in this figure represent either incident, reflected, or transmitted waves. The reflection coefficient $\Gamma$ is calculated according to (4-2), where $E_{x,amp}$ represents the amplitude of the electric field wave. An analogous equation using the incident and reflected magnetic field amplitudes would be equally valid.

$$\Gamma = 20log\left(E^r_{x,amp}/E^i_{x,amp}\right) \quad (4\text{-}2)$$

This simulation was performed varying the resolution of the coarse mesh, the refinement of the fine mesh, and the interpolation method used to obtain field values in the buffer region as per the sub-gridding algorithm. The resolution in terms of number of unit cells per wavelength of the plane wave in the coarse mesh is swept from ten to fifty. The lower limit of ten was chosen as this is the typical lower limit for conventional FDTD simulations to minimize numerical dispersion. The refinement of the fine mesh was swept among the values 3, 5, 7, and 9. The interpolation methods included linear, cubic, modified Akima cubic Hermite, and spline interpolation and were implemented using the MATLAB function interp1(). For all simulations a time step that was 0.99 times the maximum under the CFL limit was used. In terms of other simulation parameters such as the number of cells in each of the coarse mesh, fine mesh, or scattered field region, these were dependent on the number of unit cells per wavelength chosen, and care was taken to make sure that no other reflections corrupt the results of interest.

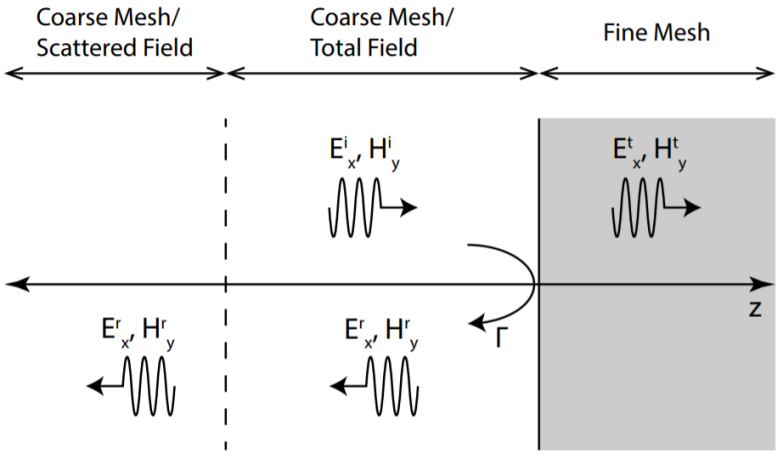


Figure 4.8: Interface reflection simulation scenario.

### 4.2.3 Simulation Results

The plots in Figures 4.9 and 4.10 show the results of this reflection test. In all cases it is seen that reflection from the coarse-fine interface decreases as the number of unit cells per wavelength increases. This is an expected result as a smaller unit cell relative to wavelength means that there is less spatial variation that could occur within the dimensions of a single unit cell. The process of interpolation for the buffer region would thus provide results more representative of the actual field variation, allowing for simulation within the extended fine mesh region to proceed with more accurate field values, making the overall coupling more accurate. In Figure 4.9, effects of sweeping the refinement are visualized. The trend in refinement and reflection coefficient is not obviously clear from these results. For example, a refinement of seven shows worse performance than a refinement of five for lower spatial resolutions, but better performance for higher resolutions. However, a refinement of nine undisputedly improves the reflection coefficient as compared to any of the smaller refinements. For each of these cases linear interpolation used for the buffer region. In Figure 4.10, a set refinement of five is chosen

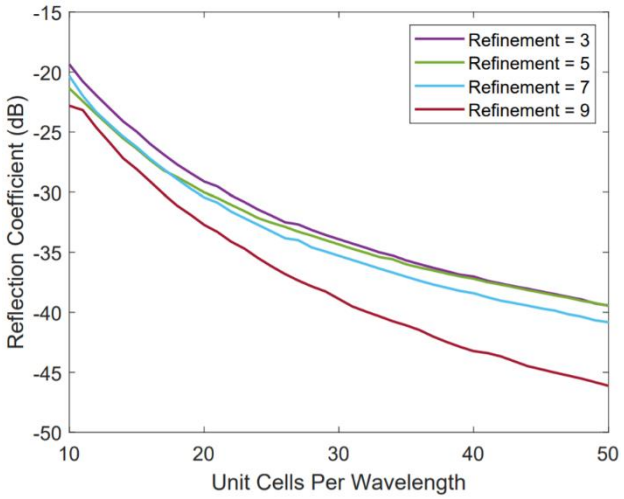


Figure 4.9: Reflection coefficient for various refinements.

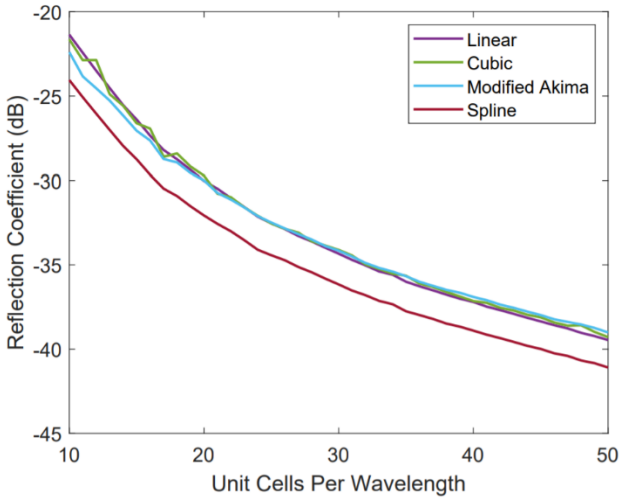


Figure 4.10: Reflection coefficient for various interpolation methods.

and the interpolation method is varied. It may be seen that spline interpolation allows for a universal improvement in terms of reducing reflection coefficient for all cases of spatial resolutions considered. Comparatively, the other interpolation methods applied have only marginal differences. Among them, linear interpolation would be the best choice in terms of accuracy with the highest computational efficiency.

## 4.3 Late Time Behavior

### 4.3.1 Motivation

In making modifications to a time domain method often certain characteristics of the modified algorithm are not obvious in simulations that terminate in a relatively short number of time iterations. Most notoriously, instability in the late time may be exhibited where field values undergo exponential growth rendering the simulation results useless. In analyzing the late time behaviors of the proposed sub-gridding method an empty resonant cavity with perfect electrically conducting walls is modeled. An intra-cavity source is used to inject a finite amount of energy in

the form of dynamic fields which is then simulated over a large number of time iterations. Due to the lack of loss mechanisms in the cavity, these fields will eventually possess some nontrivial steady state behavior. Probing the fields at some point within the cavity will then allow for this behavior to be observed, where any deviation from expectations will represent a fault in the algorithm.

### 4.3.2 Simulation Setup

The simulation scenario is presented in Figure 4.11 where a cubic cavity is modeled with dimensions of 150x150x150mm. The portion of this cavity to be discretized with a fine mesh is chosen to be a cube located at the center with dimensions of 50x50x50mm while the rest of the space is discretized with a coarse mesh. Injection of energy is accomplished with an electric line source that is z directed, 17.5 mm long, and excited with a Gaussian pulse. The spectrum of the excitation is shown in Figure 4.12 and demonstrates a center frequency of 1 GHz with a full width at half maximum of approximately 620 MHz. The source is located at the center of an xz-

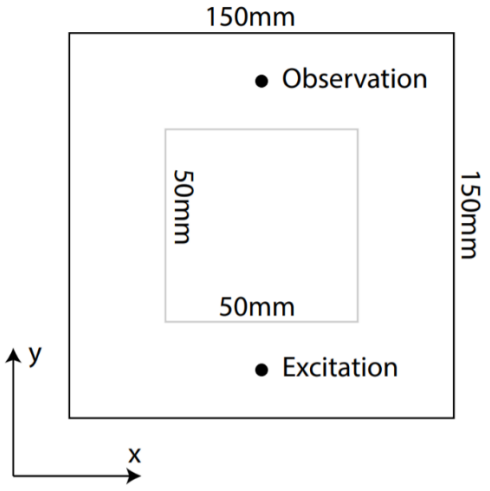


Figure 4.11: Schematic of simulation setup for resonant cavity.

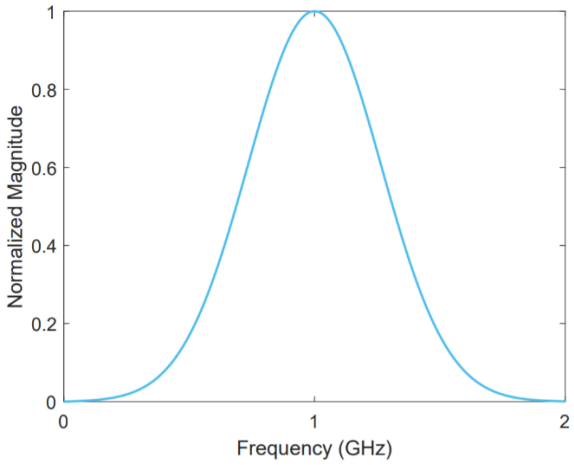


Figure 4.12: Spectrum of excitation for resonant cavity.

plane wall of the cavity and distanced 12.5 mm from this wall. The z component of the electric field is probed at an observation point centered on the opposite xz-plane wall and similarly located 12.5 mm from this wall. In discretizing the simulation space the coarse mesh had the dimensions of 60x60x60 unit cells, whereas the fine mesh had the dimensions of 60x60x60 unit cells corresponding to a refinement of three.

### 4.3.3 Simulation Results

The results visualized in Figure 4.13 and 4.14 correspond to a time step that was 0.8 times the maximum that would have been permitted by the CFL limit. Large time steps did in fact demonstrate the common problem of late time instability. However, with this empirical decrease it may be seen from Figure 4.13 that a large number of time iterations may be performed with no signs of instability. This specific plot visualizes the field value at the observation point for up to 150,000 time iterations performed. Despite the absence of late time stability, there does appear to be signs of numerical attenuation. This attenuation, while certainly a flaw of the algorithm that must be addressed in future work, is nevertheless not as catastrophic

a flaw as instability as fidelity of the waveform is maintained. To support this claim, the first 5,000 and last 5,000 time samples were taken from the observed data from Figure 4.13. These are referred to as a “early time” and “late time” portions of the measured signal respectively. A

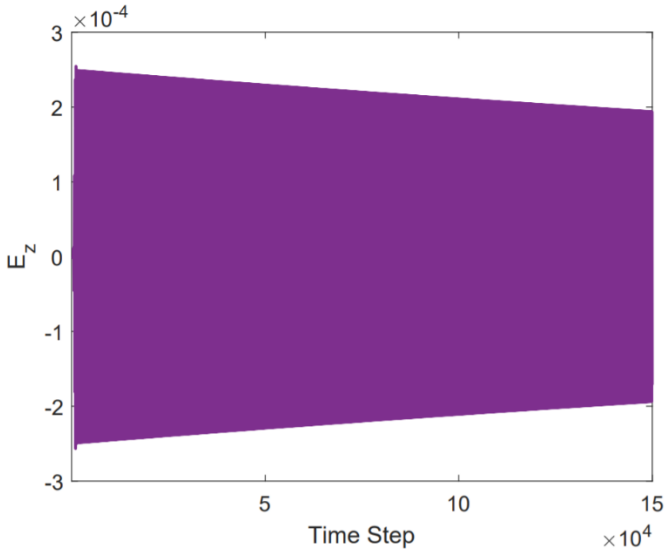


Figure 4.13: Probed field of resonant cavity.

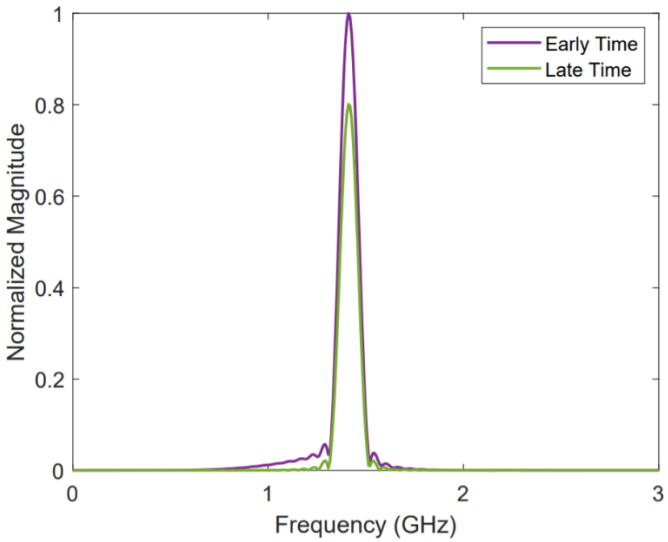


Figure 4.14: Spectrum of early and late time windows of probed field.

Hanning window is applied to each portion and the results transformed to the frequency domain using an FFT algorithm. Plotting this in Figure 4.14 demonstrates that while attenuation does occur, the spectrum of the solution is otherwise relatively unaffected, and thus the late time solution is just an attenuated version of the correct solution. Late time instability, on the other hand, does not tend to maintain the quality of the late time solution. Overall, an empirical decrease in the maximum allowed time step does seem to suppress late time instability, though the algorithm is still affected by a numerical attenuation.

# CHAPTER 5

# Conclusion and Future Work

Multi-scale simulations are inherently problematic for the conventional FDTD method. The need to resolve both small and large features results in the consumption of copious amounts of computational resources due to the requirement of uniform spatial discretization as well as the existence of the CFL limit. Uniform discretization in space causes over-resolution of large features of modeled structures and regions of space that do not experience high spatial variation of fields as a consequence of the need to resolve smaller features also present in the simulation space. The CFL limit describes the maximum time step of the simulation in order to maintain stability and is proportional to the smallest spatial feature resolved. Thus, the number of time iterations required to achieve a given time evolution of the simulation is inversely proportional to the smallest spatial feature resolved. These problems may be overcome by sub-gridding, or the introduction of local domains of fine resolution into a base domain of coarser resolution in order to resolve regions with smaller features of interest. The non-uniformity of the mesh allows for reduced memory usage, and with independent time steps used in each domain, the greatest efficiency in terms of reducing the number of computations is achieved. Past methods of sub-gridding have been consistently plagued by the lack of a combination of stability, material traverse support, and efficiency and thus none have ever been widely accepted. The proposed algorithm in this thesis represents a new approach to the sub-gridding problem. It differs from past methods primarily in its ability to obtain coarse-fine interface fields from the conventional FDTD. Numerical tests with the proposed method have validated its results and shown its

capabilities in offering improvement in the accuracy of simulating fine features while maintaining very reasonable levels of computational complexity. Testing has also shown low levels of reflection from the interface between the coarse and fine meshes that improve with overall resolution of the system. Finally, the numerical analysis of late time stability has shown that with a minor decrease in the time step with respect to the maximum according to the CFL limit, there is no late time instability evident up to 150,000 time steps.

Despite some of the successes of the proposed algorithm, there is still much future work to be done to improve its ability to be applied to general problems. For one, an analytical examination into the stability of the method is required. Without provable stability and conditions to maintain it, there is no way that the goal of a widely accepted standard sub-gridding method can be achieved. Late time instability is not as simple in origin as CFL based stability and so without knowing its source for a given algorithm, there is no way to know if it is worth applying that algorithm to some general problem. Past literature regarding the stability for sub-gridded algorithms will guide the way for this effort. Another important development is the verification of material traverse support. In theory, support for dielectric traverse is possessed by the proposed algorithm, but this has yet to be implemented. A means of treating perfect electric conductor traverse has also been yet to be developed.

Modern research problems have evolved to become highly interdisciplinary, involving phenomena from various areas of physics, yet numerical methods have not kept up. In expanding the capabilities of the FDTD method to treat such problems, the biggest hurdle is the resolution of disparate spatial scales required by the multiple physical phenomena. An efficient and general sub-gridding method is a necessary development that will undoubtedly give rise to huge leaps in the advancement of numerical methods.

# REFERENCES


[1] Huray, Paul G. Maxwell's equations. John Wiley & Sons, 2011.

[2] Ames, William F. Numerical methods for partial differential equations. Academic press, 2014.

[3] Jin, Jian-Ming. The finite element method in electromagnetics. John Wiley & Sons, 2015.

[4] Taflove, Allen, and Susan C. Hagness. Computational electrodynamics: the finite-difference time-domain method. Artech house, 2005.

[5] Taflove, Allen, Ardavan Oskooi, and Steven G. Johnson, eds. Advances in FDTD computational electrodynamics: photonics and nanotechnology. Artech house, 2013.

[6] Stiles, Paul L., et al. "Surface-enhanced Raman spectroscopy." *Annu. Rev. Anal. Chem.* 1 (2008): 601-626.

[7] Adam, J. Douglas, and Steven N. Stitzer. "Frequency selective limiters for high dynamic range microwave receivers." IEEE transactions on microwave theory and techniques 41.12 (1993): 2227-2231.

[8] Yee, Kane. "Numerical solution of initial boundary value problems involving Maxwell's equations in isotropic media." IEEE Transactions on antennas and propagation 14.3 (1966): 302-307.

[9] Ames, William F. Numerical methods for partial differential equations. Academic press, 2014.

[10] Gedney, Stephen D. "Introduction to the finite-difference time-domain (FDTD) method for electromagnetics." Synthesis Lectures on Computational Electromagnetics 6.1 (2011): 1-250.

[11] Zheng, Fenghua, Zhizhang Chen, and Jiazong Zhang. "Toward the development of a three-dimensional unconditionally stable finite-difference time-domain method." IEEE Transactions on Microwave Theory and Techniques 48.9 (2000): 1550-1558.

[12] Sun, Guilin, and Christopher W. Trueman. "Efficient implementations of the Crank-Nicolson scheme for the finite-difference time-domain method." IEEE transactions on microwave theory and techniques 54.5 (2006): 2275-2284.

[13] Shibayama, J., et al. "Efficient implicit FDTD algorithm based on locally one-dimensional scheme." Electronics Letters 41.19 (2005): 1046-1047.

[14] Zheng, Fenghua, and Zhizhang Chen. "Numerical dispersion analysis of the unconditionally stable 3-D ADI-FDTD method." IEEE Transactions on Microwave Theory and Techniques 49.5 (2001): 1006-1009.

[15] Taflove, Allen, et al. "Detailed FD-TD analysis of electromagnetic fields penetrating narrow slots and lapped joints in thick conducting screens." IEEE Transactions on Antennas and Propagation 36.2 (1988): 247-257.

[16] Umashankar, Korada R., Allen Taflove, and Benjamin Beker. "Calculation and experimental validation of induced currents on coupled wires in an arbitrary shaped cavity." IEEE Transactions on Antennas and Propagation 35.11 (1987): 1248-1257.

[17] Maloney, James G., and Glenn S. Smith. "The efficient modeling of thin material sheets in the finite-difference time-domain (FDTD) method." IEEE Transactions on antennas and Propagation 40.3 (1992): 323-330.

[18] Monk, Peter, and Endre Süli. "A convergence analysis of Yee's scheme on nonuniform grids." SIAM Journal on Numerical Analysis 31.2 (1994): 393-412.

[19] Madsen, Niel K. "Divergence preserving discrete surface integral methods for Maxwell's curl equations using non-orthogonal unstructured grids." Journal of Computational Physics 119.1 (1995): 34-45.

[20] Kunz, Karl S., and Larry Simpson. "A technique for increasing the resolution of finite-difference solutions of the Maxwell equation." IEEE Transactions on Electromagnetic Compatibility 4 (1981): 419-422.

[21] Kim, Ihn S., and Wolfgang JR Hoefer. "A local mesh refinement algorithm for the time domain-finite difference method using Maxwell's curl equations." IEEE Transactions on Microwave Theory and Techniques 38.6 (1990): 812-815.

[22] Zivanovic, Svetlana S., Kane S. Yee, and Kenneth K. Mei. "A subgridding method for the time-domain finite-difference method to solve Maxwell's equations." IEEE Transactions on Microwave Theory and Techniques 39.3 (1991): 471-479.

[23] Prescott, Deane T., and N. V. Shuley. "A method for incorporating different sized cells into the finite-difference time-domain analysis technique." IEEE Microwave and Guided Wave Letters 2.11 (1992): 434-436.

[24] Thoma, Peter, and Thomas Weiland. "A consistent subgridding scheme for the finite difference time domain method." International Journal of Numerical Modelling: Electronic Networks, Devices and Fields 9.5 (1996): 359-374.

[25] Okoniewski, Michal, Ewa Okoniewska, and Maria A. Stuchly. "Three-dimensional subgridding algorithm for FDTD." IEEE Transactions on Antennas and Propagation 45.3 (1997): 422-429.

[26] Chevalier, Michael W., Raymond J. Luebbers, and Vaughn P. Cable. "FDTD local grid with material traverse." IEEE Transactions on Antennas and Propagation 45.3 (1997): 411-421.

[27] Krishnaiah, K. M., and C. J. Railton. "Passive equivalent circuit of FDTD: An application to subgridding." Electronics Letters33.15 (1997): 1277-1278.

[28] White, Mikel J., Magdy F. Iskander, and Zhenlong Huang. "Development of a multigrid FDTD code for three-dimensional applications." IEEE Transactions on Antennas and Propagation 45.10 (1997): 1512-1517.

[29] Yu, Wenhua, and Raj Mittra. "A new subgridding method for the finite-difference time-domain (FDTD) algorithm." Microwave and optical technology letters 21.5 (1999): 330-333.

[30] Krishnaiah, K. M., and Chris J. Railton. "A stable subgridding algorithm and its application to eigenvalue problems." IEEE transactions on microwave theory and techniques 47.5 (1999): 620-628.

[31] White, Mikel J., Zhengqing Yun, and Magdy F. Iskander. "A new 3D FDTD multigrid technique with dielectric traverse capabilities." IEEE Transactions on Microwave Theory and Techniques 49.3 (2001): 422-430.

[32] Chavannes, Nicolas Pierre. Local mesh refinement algorithms for enhanced modeling capabilities in the FDTD method. Diss. ETH Zurich, 2002.

[33] Vaccari, Alessandro, et al. "A robust and efficient subgridding algorithm for finite-difference time-domain simulations of Maxwell's equations." Journal of Computational physics 194.1 (2004): 117-139.

[34] Ahmed, Iftikhar, and Zhizhang Chen. "A hybrid ADI-FDTD subgridding scheme for efficient electromagnetic computation." International Journal of Numerical Modelling: Electronic Networks, Devices and Fields 17.3 (2004): 237-249.

[35] Kulas, Lukasz, and Michal Mrozowski. "Low-reflection subgridding." IEEE transactions on microwave theory and techniques 53.5 (2005): 1587-1592.

[36] Brenger, Jean-Pierre. "A Huygens subgridding for the FDTD method." IEEE Transactions on Antennas and Propagation54.12 (2006): 3797-3804.

[37] Venkatarayalu, Neelakantam V., et al. "A stable FDTD subgridding method based on finite element formulation with hanging variables." IEEE transactions on antennas and propagation 55.3 (2007): 907-915.

[38] Chilton, Ryan A., and Robert Lee. "Conservative and provably stable FDTD subgridding." IEEE Transactions on Antennas and Propagation 55.9 (2007): 2537-2549.

[39] Kulas, Lukasz, and Michal Mrozowski. "Reciprocity principle for stable subgridding in the finite difference time domain method." EUROCON 2007-The International Conference on" Computer as a Tool". IEEE, 2007.

[40] Xiao, Kai, David J. Pommerenke, and James L. Drewniak. "A three-dimensional FDTD subgridding algorithm with separated temporal and spatial interfaces and related stability analysis." IEEE Transactions on Antennas and Propagation 55.7 (2007): 1981-1990.

[41] Berenger, Jean-Pierre. "Three dimensional Huygens subgridding for FDTD." 2009 IEEE Antennas and Propagation Society International Symposium. IEEE, 2009.

[42] Bringuier, Jonathan Neil. "Multi-scale techniques in computational electromagnetics." (2010).

[43] Ji, Ki-Man, et al. "Application of simple subgridding technique for antenna radiation patterns." Microwave and Optical Technology Letters 53.5 (2011): 1160-1162.

[44] Chang, Chun, and Costas D. Sarris. "A spatially filtered finite-difference time-domain scheme with controllable stability beyond the CFL limit: Theory and applications." IEEE Transactions on Microwave Theory and Techniques 61.1 (2013): 351-359.

[45] Li, Xihao, and Piero Triverio. "Stable FDTD simulations with subgridding at the time step of the coarse grid: A model order reduction approach." 2015 IEEE MTT-S International Conference on Numerical Electromagnetic and Multiphysics Modeling and Optimization (NEMO). IEEE, 2015.

[46] Zhou, Longjian, et al. "A hybrid method of higher-order FDTD and subgridding technique." IEEE Antennas and Wireless Propagation Letters 15 (2016): 1261-1264.

[47] Kuo, Chih-Wen, and Chih-Ming Kuo. "Finite-difference time-domain analysis of the shielding effectiveness of metallic enclosures with apertures using a novel subgridding algorithm." IEEE Transactions on Electromagnetic Compatibility 58.5 (2016): 1595-1601.

[48] Bekmambetova, Fadime, Xinyue Zhang, and Piero Triverio. "A dissipative systems theory for FDTD with application to stability analysis and subgridding." IEEE Transactions on Antennas and Propagation 65.2 (2017): 751-762.

[49] Ye, Zhihong, et al. "A novel FDTD subgridding method with improved separated temporal and spatial subgridding interfaces." IEEE Antennas and Wireless Propagation Letters16 (2017): 1011-1015.

[50] Bekmambetova, Fadime, Xinyue Zhang, and Piero Triverio. "A dissipation theory for three-dimensional FDTD with application to stability analysis and subgridding." IEEE Transactions on Antennas and Propagation 66.12 (2018): 7156-7170.

[51] Balanis, Constantine A. Advanced engineering electromagnetics. John Wiley & Sons, 1999.

[52] Marrone, Massimiliano, and Raj Mittra. "A new stable hybrid three-dimensional generalized finite difference time domain algorithm for analyzing complex structures." IEEE transactions on antennas and propagation 53.5 (2005): 1729-1737.